ROYAL SOCIETY
OF CHEMISTRY

PAPER

Check for updates

Superior solubility of anhydrous quercetin and polymer physical mixtures compared to amorphous solid dispersions†

Xu Ma,[ab] Hong Su,[b] Yongming Liu, [ID][c] Fenghua Chen [ID] *[b] and Rongrong Xue [ID] *[b]

Quercetin (QUE) is a functional flavonoid molecule with low water solubility. The study of its amorphous solid dispersions (ASDs) is still insufficient. This work reveals that the solubility of the physical mixtures of anhydrous QUE and polymers (PVP or soluplus) is better than that of the ASDs of QUE and the corresponding polymers. Gel-like phase separation occurring during the QUE ASDs dissolution process (weak in ASDs with PVP and strong in ASDs with soluplus) reduces the driving force for QUE release, which makes research on the QUE ASDs insufficient, and can be avoided in the QUE physical mixtures with polymers. Combination of metastable polymorph and polymer is a feasible strategy for improving the solubility of poorly water-soluble molecules whose ASDs encounter the gel-like phase separation.

1. Introduction

Natural products are important candidates for the prevention and treatment of diseases.[1,2] Quercetin (QUE, Scheme 1, 2-(3,4-dihydroxyphenyl)-3,5,7-trihydroxy-4H-chromen-4-one, $C_{15}H_{10}O_7$) is a natural compound that belongs to the flavonoids family and has a wide range of medical properties such as anti-inflammatory and anticancer.[3] QUE is widely present in fruits and vegetables, such as onion, fennel leaves, tea, cranberries, cherries, tartary buckwheat, *Capparis spinosa*, and others, and has been approved for widespread use as a food supplement or functional food.[4] QUE has a very low solubility in water,[5] resulting in poor bioavailability and limiting its applications. It is of great significance to prepare and select the suitable polymorphism of poorly soluble pharmaceutical compounds to improve their solubility and bioavailability.[6] More than 60% of marketed pharmaceuticals are poorly soluble, and more than two-thirds of promising new chemical entities fail to enter the clinical setting due to solubility issues.[7] Amorphous solids generally exhibit higher solubility and faster dissolution than crystalline forms.[8,9] Amorphous solid dispersion (ASDs) technology, which uses polymers as a carrier, is considered as the most promising method to solve the solubility problem of poorly soluble drugs.[10,11]

Given that QUE is one of the most studied flavonoids, it is surprising that QUE ASDs have not been reported as much (Table 1). Quercetin dihydrate (QUE-DH) is the main form sold on the market,[20] and is the main raw materials for preparing QUE ASDs. QUE-DH is not suitable for preparing QUE ASDs, especially for ball milling method,[18] because water is usually not a good component in ASDs. And the contents of QUE in the reported ASDs are not high. PVP (Scheme 1) is one of the most common used polymers in the preparations of QUE ASDs, and the QUE contents in the ASDs of QUE and PVP are not more than 25%.[14,17] Soluplus (Scheme 1) has been applied in various pharmaceutical formulations owing to its inert nature and ability to form nanomicelles.[21] Both PVP and soluplus are safe for oral, which is suitable for preparing the QUE ASDs. The ASDs of QUE and soluplus do not show a good solubility,[16] but the reason is unknown.

In this work, QUE ASDs with PVP or soloplus and their physical mixtures (PMs) were prepared to explain the insufficient reports of QUE ASDs and develop suitable formulations to improve the solubility of QUE. The solubility of the PMs of
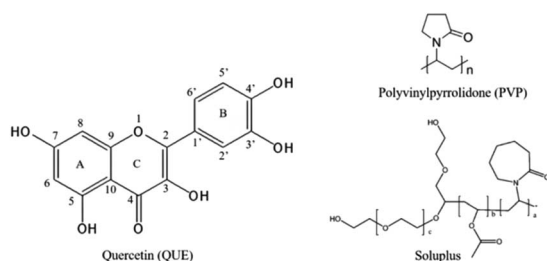
Scheme 1 Molecular structure of quercetin (QUE), polyvinylpyrrolidone (PVP), and soluplus.

[a]College of Chemistry and Materials Science, Fujian Normal University, Fuzhou, 350117, Fujian, China

[b]School of Resources and Chemical Engineering, Sanming University, Sanming, 365004, Fujian, China. E-mail: fenghuachen@fjsmu.edu.cn; rongrongxue@fjsmu.edu.cn

[c]School of Education and Music, Sanming University, Sanming, 365004, Fujian, China

Table 1 Summary of quercetin (QUE) amorphous solid dispersions (ASDs) reported in recent researches[a]

Raw QUE	Polymer	Methods	QUE content/%	Ref
Hydrate	PVP K25	Evaporating	—	12
Hydrate	Cellulose derivative	Spray dry	50	13
QUE-DH	Poloxamer 407, PEG 8000, PVP K40	Solvent evaporation, freeze drying	25	14
Mixture	Cellulose derivative	Spray dry	10	15
QUE-DH	PEG 6000, PVP VA64, soluplus, poloxamer 188	Hot melt extrusion	12.5	16
QUE-DH	HPMC-AS	Co-precipitation	10	17
QUE-DH	PVP K30	Evaporation	25	17
QUE-DH	Chitosan oligosaccharide	Ball milling	50	18
QUE-AH	PEG	Melt-mixing	40	19

[a] QUE dihydrate: QUE-DH, anhydrous QUE: QUE-AH.

anhydrous QUE (QUE-AH) and polymer is better than that of ASDs with the same QUE content and polymer. Gel-like phase separations are observed in the dissolution process of ASDs limiting the dissolution, which might be caused by the strong interactions between QUE and polymer in the ASDs which can be observed from the IR and fluorescence spectroscopy.

The PMs of metastable QUE-AH and polymer can avoid the gel-like phase separation and show a high solubility of QUE. Combination of metastable polymorph and polymer is a feasible strategy for improving the solubility of poorly water-soluble molecule.

2. Experimental section

2.1 Materials

Quercetin dihydrate (QUE-DH, $C_{15}H_{10}O_7 \cdot 2H_2O$, 97%), anhydrous quercetin (QUE-AH, $C_{15}H_{10}O_7$, 95%), and PVP K30 were purchased from Aladdin. Soluplus (repacked of the product of BASF SE) was purchased from Shanghai King Chemical. All reagents were used without treatment.

2.2 Methods

2.2.1 Macro-thermogravimetric analysis. 1.00 g of sample was added into the aluminum pan of the thermobalance (MB120ZZH, OHAUS). The mass change of the sample at a specific temperature was recorded until the sample mass no longer changed. And the water content of the sample can be calculated. Select 100 °C as the specified temperature to evaluate the sample stability under high temperature conditions. Then the dehydrated product was left in the air *in situ* (~26 °C, ~60% humidity), recorded the absorbed water within a certain time, and compared the hygroscopicity of different samples. The ambient temperature and humidity were controlled by air conditioner and dehumidifier.

2.2.2 Preparation of QUE polymorphs, ASDs and PMs. Raw QUE is QUE-DH. QUE-AH was freshly prepared by heating QUE-DH at 100 °C for 1 h. Amorphous QUE (QUE-AM) was the product obtained by ball milling of QUE-AH. QUE ASDs were prepared by neat ball milling of QUE and polymers. Totally 2 g of QUE and polymers were neat ball milled (XQM-1, 670 rpm, Tencan Powder) for 4 h. The mass concentrations of QUE in this work were 5, 10, 15, 20, 30, 40, 50, and 80%. QUE PMs (50%)

were prepared by mixing equivalent QUE polymorph and polymer with a vortex mixer (MX-S, DLAB) for 2 min.

2.2.3 Working curve of QUE aqueous solutions. ~20 mg QUE-DH (accurate to 0.1 mg) was dissolved in 1 L of deionized water at a low boiling condition. A series of QUE solutions were obtained by diluting the above solution with deionized water and then measured by ultraviolet-visible spectroscopy (UV-vis, Shimadzu UV-2550, 200–600 nm). The absorbance at 367 nm was used for linear fitting, and the working curve with a good linear was obtained in the concentration range of 0–12.5 μg mL^{-1}.

2.2.4 Solubility of QUE-DH and dissolution profiles of QUE samples. Placed 0.11 g QUE-DH at the bottom of the beaker, and added slowly 100 mL deionized water, and kept the suspension in a thermostatic water bath (37 °C or 25 °C) overnight. The supernatant without any treatment was tested by UV-vis spectroscopy. The solubility of QUE-DH can be calculated. Placed a certain mass of QUE ASDs or PMs (containing 0.10 g QUE) at the bottom of beaker, and added slowly 100 mL of deionized water (37 °C). 5 mL suspension were taken out at a certain interval of 1, 2, 4, 8, 24, 30, 48 h, and tested by UV-vis spectroscopy immediately without any treatments. Three parallel samples were tested. The dissolution profiles of QUE samples can be obtained. The static method was adopted to minimize the entry of small particles into the solution and make the supernatant suitable for UV-vis test directly.

2.2.5 Characterization. The samples were characterized by powder X-ray diffraction (PXRD, Philips X′Pert Pro, Cu Kα, 40 kV, 30 mA, 5–30°, 0.5°·min^{-1}), Fourier transform infrared spectroscopy (FTIR, Shimadzu, IRAffinity-1S, 400–4000 cm^{-1}, 2 cm^{-1}), confocal Raman spectroscopy (Thermo Fisher Scientific, DXR3xi, 532 nm, 5 mW, 0.02 s, 1000 scans, 50–3400 cm^{-1}), fluorescence spectroscopy (FL, Gangdong Technology, F-320A, 500–640 nm) and scanning electron microscope (SEM, Thermo Fisher Scientific Apreo 2C, 5 kV).

3. Results

3.1 Stability, hygroscopicity and solubility of QUE

QUE is generally considered as a molecule with poor stability.[22] It is essential to ensure the stability of QUE during the formulation preparation. The macro-thermogravimetric curve of

commercial QUE-DH shows a weight loss of 9.7% within 30 minutes in air at 100 °C (Fig. 1a), which is close to the theoretical water content 10.7% of QUE-DH. The mass of QUE after dehydration tends to be constant, indicating that QUE has good thermal stability under the experimental condition.[23] If heated in air to the temperature up to 150 °C, the mass of sample still decreases after the loss of water (Fig. S1†), indicating a slight oxidation or decomposition of QUE molecules.[24] The commercial PVP and soluplus are also stable at 100 °C (Fig. 1a), with the water adsorbed during storage lost, the water content of PVP and soluplus is 5.4% and 3.6%, respectively.

The moisture absorption processes of QUE-AH, dry PVP and soluplus at room temperature and ambient humidity of ∼60% were monitored (Fig. 1b). The moisture absorption capacity of QUE-AH is weak, and the absorbed water content was 0.8% in 90 minutes and 1.7% (Fig. S2†) in one week, respectively, which indicates that the conversion from QUE-AH to QUE-DH is slow in air. PVP and soluplus, especially PVP, have a faster moisture absorption rate and a stronger moisture absorption capacity than QUE-AH. The absorbed water content of PVP was up to 10% in 90 minutes, and that of soluplus reached 2.3%.

The aqueous solubility of QUE is puzzling. The measured solubility of QUE at 25 °C ranges from 0.39 to 920 μg mL^{-1},[25–27] and the computational or fitted values are in the range from 3.2 to 38 μg mL^{-1}.[5,28] The solubility of poorly soluble molecules is easy to be influenced by various factors including measurement method (ultrasonic,[29] suspension time,[30] and filtration) and reagents (polymorph, purity, and stability[31] *etc.*). The typical process of QUE solubility measurement including supernatant

preparation, supernatant treatments (filtrated with membranes and diluted with organic solvents), working curve establishment of UV-visible spectroscopy or HPLC method, and concentration test. QUE solubility measurement was proposed here by using UV-visible spectroscopy and aqueous working curve, because the dilution with organic solvents and HPLC method can dissolve the QUE nanoparticles which would interfere with the test accuracy. The QUE aqueous solution was stable within 3 days (Fig. S3†). QUE-DH was used to prepare the standard solutions due to its stability and low-hygroscopic, and the QUE concentration was calculated based on the macro-thermogravimetric result (Fig. 1a). The UV-vis spectra of QUE solutions (Fig. S4†) are similar as the reported ones,[32] and the absorption of the solutions at 367 nm showed a good linear relationship with its concentration in the range of 1.8–12.5 μg mL^{-1}. The working curve of QUE aqueous solutions was established (Fig. 1c) for the non-destructive UV-vis spectroscopy test of QUE, whose molar absorption coefficient is only ∼80% of that of QUE 50 vol% water–ethanol solutions (Fig. S5†). The QUE concentration would decrease significantly after the QUE aqueous solution filtrated with PES membranes (Fig. 1d), each filtration process causing approximately a 0.10 decrease of the absorbance (equivalent to a concentration decrease of 3 μg mL^{-1}), which is critical for the accurate determination of QUE solubility, thus, in this work a static method was employed to minimize the entry of small particles into the solutions to make the supernatant suitable for the UV-vis spectroscopy tests directly. The aqueous solubility of QUE-DH tested by this method is 3.5 ± 0.2 μg mL^{-1} at 25 °C and 6.7 ± 0.2 μg mL^{-1} at 37 °C.

We think that the method proposed in this work has the following advantages. (I) The method is simple, consistent with the Occam's razor principle. (II) The solvent used is only water. There is no issue of different molar coefficients in different solvents and the dissolution of insoluble QUE particles. (III) QUE aqueous solubility in the common temperatures must be included in the range of working curve, providing a valuable reference for the accuracy of solubility measurements.

3.2 Preparation and characterizations of three QUE polymorphs

3.2.1 Preparation of three QUE polymorphs. Three QUE polymorphs, QUE-DH, QUE-AH, and amorphous QUE (QUE-AM), were prepared and characterized. The commercial QUE can be QUE-DH or QUE-AH. QUE-DH is the most stable form under normal condition (25 °C, 50–60% humidity).[23] Commercial QUE used in this work is QUE-DH, which was confirmed by the PXRD test,[20] and no other QUE phases were detected (Fig. 2a). The typical 2θ peak of QUE-DH are at 10.7°, 12.4° and 27.3°. QUE-DH after being neat ball milled only showed the characteristic diffraction peaks at 10.6°, 12.3°, and 27.3°. Moreover, the peak positions have a little left-shift and the peak widths at half-height increase significantly compared to QUE-DH, indicating a little increase of *d*-spacing and a marked reduction of crystals size during the ball milling process, and suggesting the ball milled QUE-DH is a poorly crystalline QUE-
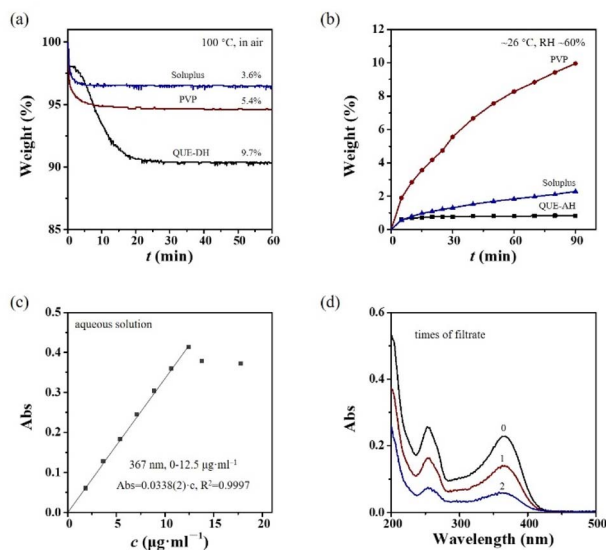

Fig. 1 Hygroscopicity and solubility of QUE. (a) Macro-thermogravimetric curve obtained by monitoring the dehydration processes of QUE-DH, raw PVP, and soluplus at 100 °C in air, (b) hygroscopicity of QUE-AH, dry PVP and soluplus at room temperature and ∼60% humidity, (c) the fitted working curve of QUE aqueous solutions in the concentration range of 0–12.5 μg mL^{-1} (consistent with Lambert–Beer's law), (d) UV-vis spectra of QUE saturated aqueous solution at 37 °C with different filtration times.
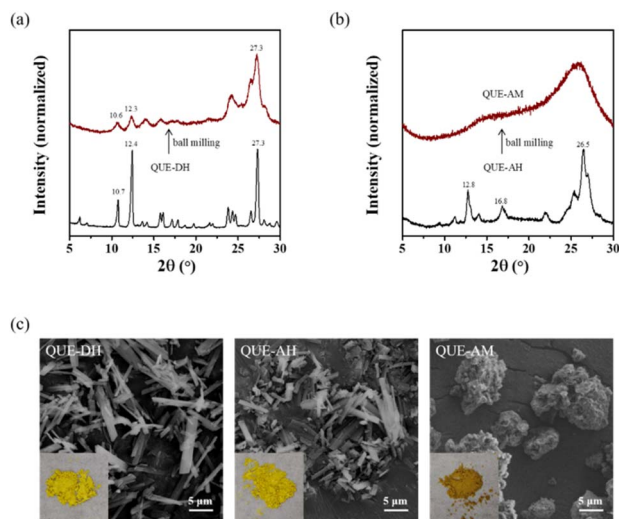
Fig. 2 Preparation of three QUE polymorphs. The PXRD patterns of (a) QUE-DH (raw QUE) and ball milled QUE-DH, (b) QUE-AH obtained by heating QUE-DH at 100 °C in air for 1 hour and amorphous QUE (QUE-AM) prepared through ball milling of QUE-AH. And (c) optical and SEM images of QUE-DH, QUE-AH and QUE-AM.
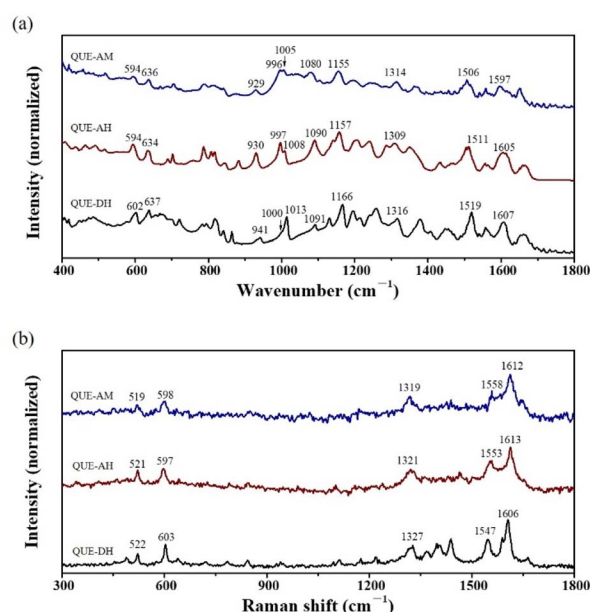

Fig. 3 Vibrational spectra of QUE-DH, QUE-AH, and QUE-AM. (a) IR, and (b) mid-frequency Raman spectra (in the range of 300–1800 cm^{-1}).

DH with defects and disorders, which is consistent with the reported result.[18]

The commercial QUE-AH transformed into QUE-DH after years' storage (Fig. S6†). Fresh QUE-AH was prepared by heating QUE-DH in air at 100 °C for 1 hour, and its PXRD pattern shows the characteristic diffraction peaks at 12.8°, 16.8°, and 26.5° (Fig. 2b), which is same as that of the reported raw QUE-AH[19] and the dehydration product of QUE-DH.[23] The peak widths at half-height of QUE-AH are broader than those of QUE-DH, indicating a crystallinity decrease during the dehydration process.

QUE-AM was the product of neat ball milling of QUE-AH. The PXRD pattern of QUE-AM has no obvious diffraction peaks, only showing very broad humps, which is the characteristic of amorphous phase. To our best know, the complete amorphization of QUE has not been reported yet.

The optical and SEM images of QUE-DH, QUE-AH and QUE-AM are shown in Fig. 2c. QUE-DH, QUE-AH and QUE-AM are all powders. QUE-DH and QUE-AH are light yellow, and QUE-AM is brown yellow. QUE-DH is micro rod-like crystals observed from the SEM image, and the morphology of QUE-AH is similar as that of QUE-DH. There are some cracks observed in the micro rod-like crystals of QUE-AH, which may be caused by the dehydration process. QUE-AM is micro irregular particles composed of small particles.

3.2.2 Vibrational spectra comparison of the three QUE polymorphs. Vibrational spectra (IR and Raman) of QUE-DH, QUE-AH, and QUE-AM are shown in Fig. 3. The spectra of them are similar overall because they contain the same QUE molecules, and most of the signals can be correlated with each other. Empirically, the difference of band locations >4 cm^{-1} for IR spectroscopy and >2 cm^{-1} for Raman spectroscopy can be regarded as distinguishing features among various polymorphs.

For QUE, IR spectra in the fingerprint region (400–1800 cm^{-1}) can be used to distinguish different phases with abundant signals, while IR spectra in the range of 2600–3600 cm^{-1} are not suitable due to the very broad peak at 3300 cm^{-1} of hydroxyl groups (Fig. S7†). The IR peaks of QUE are abundant and numerous, for the purpose of convenient comparison, 10 IR peaks of QUE-AM (Fig. 3a and Table 2) were assigned[33] and selected for polymorphs comparison because of their relative strong intensities. The characteristic peaks of QUE-AM are at 1080, 1506, and 1597 cm^{-1}, QUE-AH are at 1309 and 1511 cm^{-1}, and QUE-DH are at 602, 941, 1013, 1166, and 1519 cm^{-1}, respectively, which can be used for identified them.

Raman spectra of QUE have a poor signal-to-noise ratio and show few signals (Fig. 3b). Low-frequency Raman spectroscopy is usually a fast method to identify polymorphs,[34] but QUE polymorphs cannot be identified due to their poor signal-to-noise ratio (Fig. S8†). Raman spectra of QUE in literature sometimes shows a poor signal-to-noise ratio and sometimes has a relatively good signal-to-noise ratio,[35,36] which might be caused by the impurity of QUE. QUE molecule contains a lot of hydroxyl group, its Raman activity is not strong, the presence of fluorescence also makes it difficult to obtain its high-quality Raman spectra, and moreover, QUE is not stable under laser due to its instability. 5 typical bands in the mid-frequency Raman spectra (in the range of 300–1800 cm^{-1}) of QUE are listed (Table S1†), however, it is failed to distinguish QUE polymorphs based on the current poor signal-to-noise ratio.

The IR and Raman spectra can be used for explaining from structure why QUE-AM can be obtained from QUE-AH instead of QUE-DH through neat ball milling. 6 among the 10 IR peaks selected (594, 636, 929, 996, 1005, 1155 cm^{-1}) of QUE-AM cannot be distinguished from QUE-AH, while only 3 IR peaks

Table 2 IR peaks (cm^{-1}) and assignments of QUE polymorphs[a]

IR peaks (cm^{-1})

AM	AH	DH	Assignments
594	594	602	$\gamma(C) + \gamma(A) + \delta(COH)_{A5} + \delta(COH)_{B3',4'} + \omega(COH)_{A7} + \gamma(B)$
636	634	637	$\gamma(C) + \gamma(A) + \delta(C{=}O)$
929	930	941	$\gamma(B) + \gamma(A) + \nu(C{-}O)_{C3} + \delta(C{=}O) + \nu(C{-}O)_{B3'}$
996	997	1000	$\delta(A) + \delta(B) + \delta(CH)_{A6,8}$
1005	1008	1013	$\delta(A) + \delta(C) + \delta(B) + \delta(CH)_{A6,8}$
1080	1090	1091	$\delta(C) + \delta(A)$
1155	1157	1166	$\delta(CH)_{A8} + \delta(OH)_{A7} + \delta(A)$
1314	1309	1316	$\nu(B) + \delta(OH)_{B4'}$
1506	1511	1519	$\nu(A) + \delta(OH)_{A5} + \delta(CH)_{A8} + \nu(C{-}O)_{A7}$
1597	1605	1607	$\nu(A) + \nu(C) + \nu(C{=}O)$

[a] In-plane vibrations: ν – stretching; δ – bending; out-of plane vibrations: γ – torsional; ω – wagging vibrations; A – phenyl ring in chromone, B – phenyl ring, C – pyrone ring.[33]

(636, 996, 1314 cm^{-1}) of QUE-AM are similar as those of QUE-DH. 4 among 5 Raman bands selected (519, 598, 1319, 1612 cm^{-1}) of QUE-AM are similar as those of QUE-AH, and no band of QUE-AM is similar as that of QUE-DH. Both IR and Raman spectra indicate that the structure of QUE-AM is more similar to that of QUE-AH than QUE-DH. Thus, we proposed that the polymorph transition from QUE-AH to QUE-AM is easier than that from QUE-DH to QUE-AM based on their structure similarity.

3.2.3 Dissolution property of the three QUE polymorphs. The dissolution profiles of QUE-DH, QUE-AH and QUE-AM are shown in Fig. 4a. QUE-DH has a typical dissolution profile of stable crystalline form, it dissolves into the media slowly, and the concentration of QUE increases gradually. The concentration of QUE reaches the maximum (6.7 ± 0.2 μg mL^{-1}) at 8 h, and remains constant until 48 h. Differently, QUE-AH and QUE-AM show typical dissolution profiles of metastable form. For QUE-AH, it achieves the maximum QUE concentration of 17.0 ± 1.2 μg mL^{-1} (2.5 times the solubility of QUE-DH) within 2 hours. Subsequently, the QUE concentration decreases rapidly, and is 13.8 ± 0.1 μg mL^{-1} at 8 h, and 8.4 ± 0.3 μg mL^{-1} (supersaturation $S = 0.3$) at 24 h, respectively. For QUE-AM, the QUE concentration is 23.3 ± 1.2 μg mL^{-1} at 1 h and 22.5 ± 1.0 μg mL^{-1} at 2 h (3.4 times the solubility of QUE-DH), respectively. And the QUE concentration decreases to 13.4 ± 0.4 μg mL^{-1} at 8 h and 9.0 ± 0.5 μg mL^{-1} ($S = 0.3$) at 24 h. QUE-AH and QUE-

AM cannot maintain a high supersaturation in aqueous environments, indicating the recrystallization from QUE-AH and QUE-AM to QUE-DH. It is necessary to inhibit this recrystallization process to make QUE-AH and QUE-AM suitable as QUE formulations.

The stability order is QUE-DH > QUE-AH > QUE-AM, which can be concluded from above dissolution profiles. Theoretically, QUE-DH and QUE-AH are stable under sealed storage condition. QUE-AM can maintain amorphous state for 7 days with sealed storage condition, and would slightly recrystallize into QUE-AH (with characteristic diffraction peaks at 12.9° and 26.6°) after 30 or 60 days' storage (Fig. 4b). Although QUE-AM primarily remained amorphous after storage, the stability of QUE-AM prepared by neat ball milling of QUE-AH was not enough to support its use as a pharmaceutical formulation.

3.3 Preparation and characterizations of QUE ASDs

3.3.1 Solubilizing effect of PVP and soluplus on QUE-DH. ASDs technology was used to stabilize QUE-AM. Polymer PVP and soluplus, which are widely used in the preparation of drugs ASDs, were used in this work. The solubilizing effect of PVP and soluplus on QUE-DH was compared firstly. PVP and soluplus aqueous solutions (1 mg mL^{-1}, Fig. S9†) do not have absorbance at 367 nm, indicating the existing of these polymers do not interface the measurements of QUE concentrations. PVP shows a limited solubilizing effect on QUE-DH, the solubility of QUE-DH at 37 °C is 7.8 ± 0.2 μg mL^{-1} with PVP concentration of 0.1 mg mL^{-1} and 10.6 ± 0.1 μg mL^{-1} with PVP concentration of 1.0 mg mL^{-1} (Fig. 5a). Soluplus has significant solubilization effect because of its ability to form micelles. The critical micelle concentration of soluplus is 7.6 μg mL^{-1} (Soluplus®. BASF Technical Information, 2019). When the concentration of soluplus was 0.01 mg mL^{-1}, slightly above its critical micelle concentration, the solubility of QUE-DH was 7.1 ± 1.0 μg mL^{-1} (Fig. 5b). When the concentration of soluplus was increased to 0.1 or 1.0 mg mL^{-1}, the solubility of QUE-DH increased to 27.6 ± 1.7 or 60 ± 2 μg mL^{-1}, respectively, demonstrating a marked solubilizing effect. Soluplus has a stronger solubilization effect
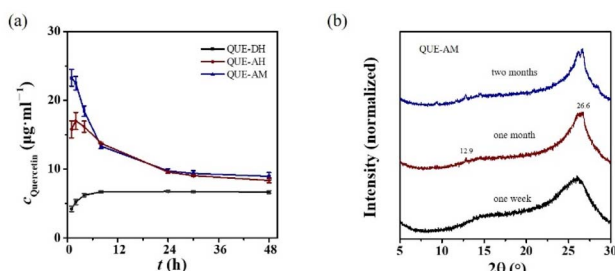

Fig. 4 (a) Dissolution profiles of QUE polymorphs at 37 °C, (b) PXRD patterns of QUE-AM after stored for a certain time.
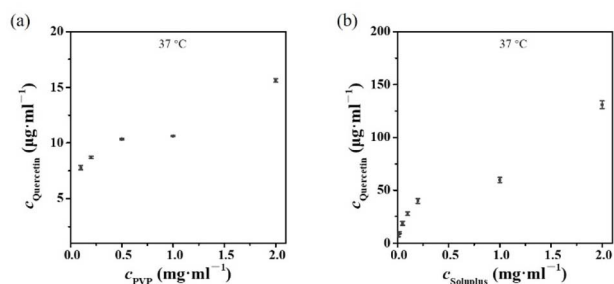
Fig. 5 Solubilities of QUE-DH at 37 °C with different (a) PVP and (b) soluplus concentrations.

on QUE than PVP, thus, soluplus might be more suitable than PVP in the preparation of QUE ASDs.

3.3.2 Preparation and characterizations of QUE ASDs with PVP. A series of QUE ASDs with PVP (BM-PVP) were prepared by neat ball milling of the mixtures of QUE-AH and PVP. The PXRD patterns of BM-PVP with the QUE content in the range from 0.1 to 0.8 (BM-PVP-ω_{QUE}, Fig. 6a) mainly show the amorphous characteristics. A weak diffraction peak at 26.6° was observed in the PXRD patterns of BM-PVP-0.8 and BM-PVP-0.5, corresponding to the signal of QUE-AH. The signal becomes barely observable when the QUE content is below 0.5. There was no significant change of the PXRD patterns of BM-PVP after sealed stored for 90 days, indicating the good stability of the BM-PVP.

Under the dissolution experiment condition, the PVP concentrations of samples BM-PVP-0.5, BM-PVP-0.2, and BM-PVP-0.1 are 0.1, 0.4, and 0.9 mg mL^{-1}, respectively. The dissolution profiles of BM-PVP samples at 37 °C (Fig. 6b) show that all of them could maintain the supersaturated concentration of

QUE within 48 h. The QUE concentration at 48 h of BM-PVP-0.8 is 10.9 ± 0.7 μg mL^{-1}, indicating that this PVP content is insufficient to stabilize QUE-AM. And the QUE concentrations at 48 h of BM-PVP-0.5, BM-PVP-0.4, and BM-PVP-0.3 were close, which are 25.5 ± 1.0, 30.6 ± 0.8, and 39.3 ± 0.8 μg mL^{-1}, respectively. The amount of PVP (>0.5) contained in these three samples can effectively inhibit the recrystallization of QUE-AM. The QUE concentration at 48 h of BM-PVP-0.2 can be up to 77 ± 7 μg mL^{-1}, which is significantly higher than that of BM-PVP-0.3. BM-PVP-0.1 completely dissolved once deionized water was added in the dissolution experiment. However, during the dissolution process, unlike other BM-PVP systems, some orange flakes were observed (Fig. 6c) in the BM-PVP-0.2 and BM-PVP-0.1 systems, which might be attributed to the oxidation of QUE.

The dissolution profiles of BM-PVP could be explained by structure characterizations. After careful comparisons of the IR and Raman spectra of QUE-AM, BM-PVP and PVP (Fig. 3 and S10†), we found that most of the IR and Raman signals remain unchanged, and only the IR peak at 1155 cm^{-1} (corresponding to the vibrational mode of $\delta(CH)_{A8} + \delta(OH)_{A7} + \delta(A)$) has a notable shift (>8 cm^{-1}). The vibrational mode of $\delta(OH)_{A7}$ is related to the interaction between the hydroxyl group at A7 position of QUE and PVP. As the QUE contents of BM-PVP decrease, a significant red shift of $\delta(OH)_{A7}$ is observed (Fig. 7a), indicating that the hydrogen bond between QUE and PVP become strong. A good linear relationship between the peak position of $\delta(OH)_{A7}$ and the QUE content is observed for BM-PVP with the QUE content in the range of 0.05–0.8 (Fig. 7b), which can be used to roughly estimate the QUE contents in the ASDs.
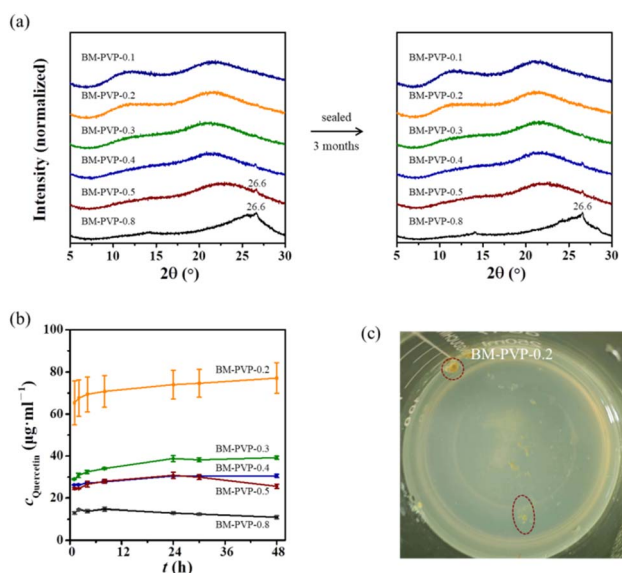

Fig. 6 Preparations and the dissolution profiles of QUE ASDs with PVP (BM-PVP). (a) PXRD patterns of BM-PVP freshly prepared (left) and stored for 90 days (right), (b) dissolution profiles at 37 °C, and (c) optical image of the suspension of BM-PVP-0.2 at 24 h during the dissolution process.
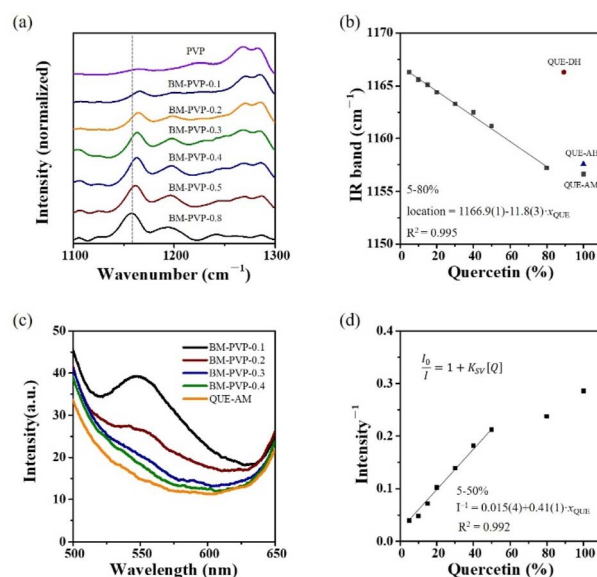

Fig. 7 Structure characterizations and data fittings of BM-PVP. (a) IR spectra in the range of 1100–1300 cm^{-1}, (b) locations and the fitted curve against the QUE contents of the IR peak corresponding to the peak at 1155 cm^{-1} of QUE-AM, (c) fluorescence emission spectra (λ_{ex} = 350 nm), (d) fluorescence intensities and the fitted curve against the QUE contents.

$\delta(OH)_{A7} = 1167-12 \cdot x_{QUE}$ $(0.05 \leq x_{QUE} \leq 0.8)$, $R^2 = 0.995$.

The molecular weight of QUE is 302 g mol^{-1}, and PVP K30 is ~40 000. When the molar ratio of QUE to PVP is 1 : 1, the mass fraction of QUE is 0.8%, which is much lower than that of BM-PVP prepared in this work. When the QUE content of BM-PVP is high, the mainly existence form of QUE is amorphous particles, and the interaction between QUE molecules is the main interaction in BM-PVP. As the QUE content decreases, the interactions between QUE and PVP become more, and the interactions between QUE molecules become less.

Fluorescence spectroscopy can be utilized to analyze the molecule existence form of QUE in its ASDs. QUE-DH and QUE-AH have fluorescence (Fig. S11†),[37,38] and QUE-AM does not have fluorescence. BM-PVP-0.4 and BM-PVP-0.3 have negligible fluorescence, whereas BM-PVP-0.2 has observable fluorescence, and BM-PVP-0.1 shows pronounced fluorescence (Fig. 7c). According to the ACQ phenomenon, the emergence of fluorescence of QUE ASDs means the formation of solid dispersions with QUE existing in molecular form (referred as molecular solid dispersions).

The ACQ phenomenon can be fitted with the Stern–Volmer equation.

$$I_o I^{-1} = 1 + K_{SV}[Q]$$

I_o is the fluorescence intensity in the absence of the quencher (Q), and I is the fluorescence intensity in the presence of the quencher at a given concentration. K_{SV} is the Stern–Volmer quenching constant. A higher value of K_{SV} indicates a more efficient quenching. $[Q]$ is the concentration of the quencher. The reciprocal of fluorescence intensity of BM-PVP shows a good relationship with x_{QUE} (in the range of 0.05–0.5) (Fig. 7d).

$$I^{-1} = 0.015 + 0.41 \cdot x_{QUE} \quad (0.05 \leq x_{QUE} \leq 0.5), R^2 = 0.992.$$

The fluorescence spectra of BM-PVP indicate that molecular solid dispersions of QUE become pronounced when $x_{QUE} \leq 0.2$. We think that the emergence of molecular solid dispersions can significantly improve the solubility, which is confirmed by the higher solubility of BM-PVP-0.2. However, molecular solid dispersions are more readily oxidized than ASDs, as observed during the dissolution process of BM-PVP-0.2 (appearance of the orange flakes). Although BM-PVP-0.1 and BM-PVP-0.2 show a superior dissolution property, they are not suitable for ASDs application. Considering the dissolution performance and stability, BM-PVP-0.5, BM-PVP-0.4, and BM-PVP-0.3 are suitable candidates as ASDs.

3.3.3 Preparation and characterizations of QUE ASDs with soluplus.
Since soluplus exhibits a superior solubilization effect on QUE-DH, the ASDs of QUE with soluplus (BM-soluplus) were prepared *via* neat ball milling of QUE-AH and soluplus, which was expected to have better properties. The PXRD patterns of BM-soluplus with the QUE content in the range from 0.1 to 0.8

(BM-soluplus-ω_{QUE}), with no any observable diffraction peaks, confirm their completely amorphous feature (Fig. 8a). PXRD test was carried out for BM-soluplus after they were sealed stored for 90 days, there was no significant change in the PXRD patterns of BM-soluplus-0.1, BM-soluplus-0.2, BM-soluplus-0.3 and BM-soluplus-0.4, and a weak peak at 26.5° appeared for BM-soluplus-0.5 and BM-soluplus-0.8, indicating a relatively good stability of the QUE ASDs with soluplus.

Unfortunately, the dissolution profiles of BM-soluplus show that the QUE concentration are less than 8 μg mL^{-1} over 24 h (Fig. 8b). The apparent solubility of BM-soluplus-0.2 at 24 h is only 1.7 μg mL^{-1}, significantly lower than the solubility of QUE-DH. We found that a gel-like phase separation (Fig. 8c) happened immediately once BM-soluplus-0.2 was added into water. Therefore, soluplus is not suitable for the preparation of the ASDs of QUE.

The peak corresponding to the $\delta(OH)_{A7}$ of BM-soluplus gradually red shift with the increase of soluplus content (Fig. 9a). And the peak position of $\delta(OH)_{A7}$ show a good linear relationship (Fig. 9b) with the content of QUE (from BM-PVP-0.1 to QUE-AM).

$$\delta(OH)_{A7} = 1168-12 \cdot x_{QUE} \quad (0.1 \leq x_{QUE} \leq 1), R^2 = 0.997.$$

Compared with BM-PVP, BM-soluplus exhibits a higher peak position of $\delta(OH)_{A7}$ at the same QUE concentration, indicating a stronger binding interaction between QUE and soluplus.

BM-soluplus-0.4 does not show any fluorescence signal, while BM-soluplus-0.3 displays a significant fluorescence signal (Fig. 9c). Compared with BM-PVP, the emergence of molecular solid dispersions of QUE is at a higher QUE concentration,
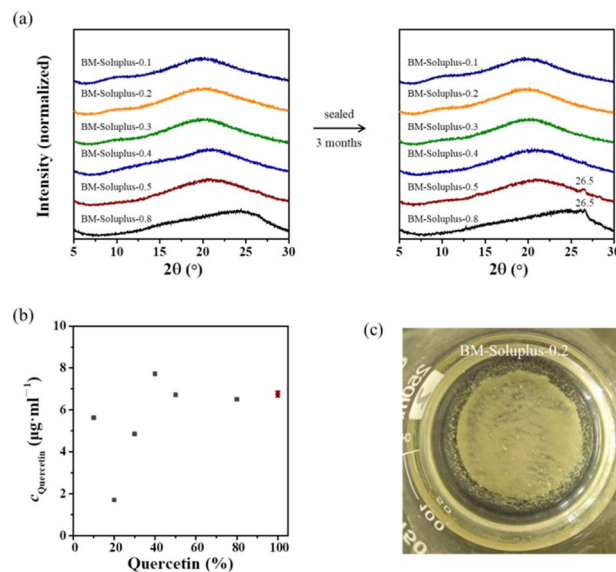

Fig. 8 Preparations and the apparent solubility of QUE ASDs with soluplus (BM-soluplus). (a) PXRD patterns of BM-soluplus freshly prepared (left) and sealed stored for 90 days (right), (b) the apparent solubility of BM-soluplus at 37 °C, (c) optical image of the suspension of BM-soluplus-0.2 at 24 h during dissolution process.
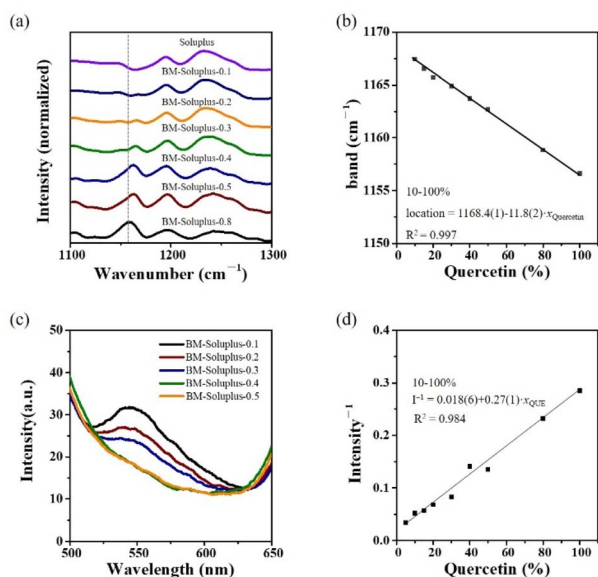
Fig. 9 Structural characterizations and the data fittings of BM-soluplus. (a) IR spectra, (b) locations and the fitted curve against the QUE contents of the IR peak corresponding to the peak at 1155 cm^{-1} of QUE-AM, (c) fluorescence emission spectra (λ_{ex} = 350 nm), (d) fluorescence intensities and the fitted curve against the QUE contents.

Fig. 10 Preparations and dissolution profiles of the physical mixtures (PMs) of the three QUE polymorphs with PVP or soluplus (PM–PVP–QUE polymoph or PM–soluplus–QUE polymoph). (a) PXRD patterns and (b) dissolution profiles of PM–PVP, (c) PXRD patterns and (d) dissolution profiles of PM–soluplus.

which confirms the stronger binding interaction between QUE and soluplus.

The fluorescence intensity of BM-soluplus against the content of QUE is well fitted with the Stern–Volmer equation (Fig. 9d).

$$I^{-1} = 0.018 + 0.27 \cdot x_{QUE} \ (0.1 \leq x_{QUE} \leq 1), \ R^2 = 0.984.$$

The K_{SV} of BM-soluplus is smaller than that of BM-PVP, indicating a less efficient quenching, which means that the interaction between QUE molecules in BM-soluplus is weaker than that in BM-PVP. Conversely, the interaction between QUE and polymer in BM-soluplus is stronger than that in BM-PVP.

3.4 Characterizations of physical mixtures of the three QUE polymorphs with PVP or soluplus

Physical mixtures (PMs) are commonly used as the reference samples in the ASDs field to demonstrate the superior efficacy of the ASDs. QUE-AH and QUE-AM are metastable forms, which can be stabilized by polymers. The apparent solubility of QUE-AH and QUE-AM can be maintained at a high level in the presence of polymers, which can prevent the occurrence of gel-like phase separation as in QUE ASDs.

The PXRD patterns of the PMs of the three QUE polymorphs with equivalent PVP (PM-PVP, named as PM-PVP-QUE polymorph) show that QUE-AH and QUE-AM maintain their structure after physically mixed with PVP, while QUE-DH transforms into QUE-AH completely (Fig. 10a). Thus, PM-PVP-QUE DH (PM-PVP-DH) and PM-PVP-QUE AH (PM-PVP-AH) are the mixtures of QUE-AH and PVP with different water contents.
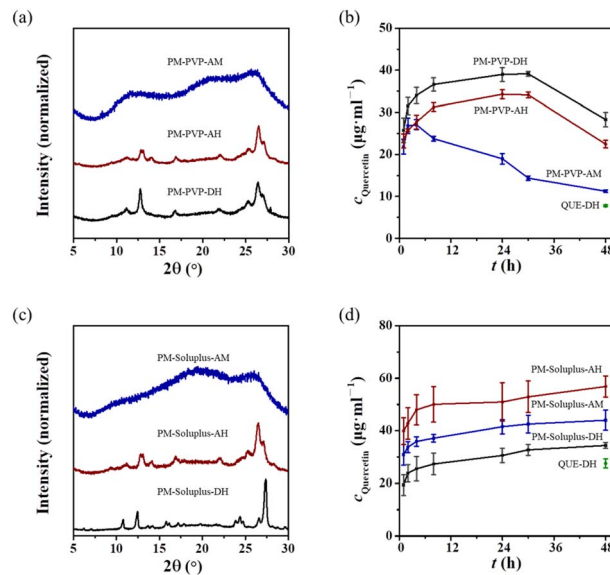
The dissolution profiles of PM-PVP-DH and PM-PVP-AH do not have significant difference with a deviation less than 10% (Fig. 10b). The apparent solubility of PM-PVP-AH (30.6 ± 0.8 μg mL^{-1} at 48 h) is 20% higher than that of BM-PVP-0.5, indicating that the PM-PVP has a slightly improved performance compared with the ASDs. The dissolution profile of PM-PVP-QUE AM (PM-PVP-AM) is better than that of QUE-AM, but still encounters the recrystallization of QUE-AM, with its apparent solubility continuously decreasing (11.2 ± 0.3 μg mL^{-1}, similar as that of QUE-AM). Theoretically, the solubility of QUE ASDs is superior to that of QUE-AH. While BM-PVP-0.5 has a significant solubilization effect on QUE, it may be confronted with the problem of gel-like phase separation, which leads to a solubility performance inferior to PM-PVP-AH.

The PMs of the three QUE polymorphs with equivalent soluplus (PM-soluplus, named as PM-soluplus-QUE polymorph) do not show significant polymorphism transformation (Fig. 10c). The apparent solubility of PM-soluplus-DH (34.3 ± 1.2 μg mL^{-1} at 48 h) is slightly higher than that of QUE-DH (27.6 ± 1.7 μg mL^{-1}) with the same concentration of soluplus (Fig. 10d), which might be caused by soluplus absorbing water from QUE-DH owing to its hygroscopicity. The overall dissolution profiles indicate that the order of solubilization is PM-soluplus-AH > PM-soluplus-AM > PM-soluplus-DH. The apparent solubility of PM-soluplus-AH (57 ± 4 μg mL^{-1} at 48 h) achieves an 8.5-fold increase compared to QUE-DH and a 2.1-fold increase compared to QUE-DH with the same concentration of soluplus.

IR spectroscopy was utilized to determine the existing form of QUE in the PMs (Fig. 11). Briefly, QUE polymorphs can be identified by their characteristic peaks: 1080, 1506, 1597 cm^{-1} of QUE-AM, 1309, 1511 cm^{-1} of QUE-AH, and 602, 941, 1013, 1166, 1519 cm^{-1} of QUE-DH. The presences of peaks at 1310
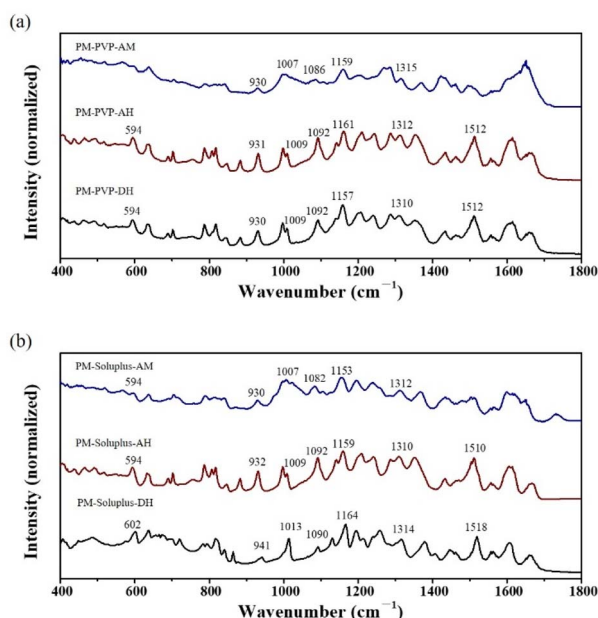
Fig. 11 IR spectra of (a) PM-PVP and (b) PM-soluplus.

and 1512 cm^{-1} of PM-PVP-DH indicate the presence of QUE-AH (differences <4 cm^{-1}), with no signal of QUE-AM and QUE-DH, suggesting a complete transformation from QUE-DH to QUE-AH during mixing. PM-PVP-AH only shows the IR peaks at 1312 and 1512 cm^{-1}, confirming the existence of QUE-AH. The characteristic IR peak at 1082 cm^{-1} of PM-PVP-AM identifies its amorphous feature. IR spectra do not show a strong interaction between QUE and PVP or soluplus, indicating the existence form of QUE in PMs is particles.

The optical images of the PMs samples (Fig. 12) are different from those of ASDs. PVP and soluplus are white powders exhibiting pronounced granularity. BM-PVP-0.5 and BM-soluplus-0.5 are brown yellow, and the colour of BM-soluplus-0.5 is deeper than that of BM-PVP-0.5, which might be caused by the strong interaction between QUE and soluplus. PM-PVP-AH and PM-soluplus-AH are light yellow similar to that of

QUE-AH, indicating that QUE-AH does not change during the physical mixing process. There are some aggregated spheres existed in PM-PVP-AH and PM-soluplus-AH, which might be caused the physical adhesions.

As shown in the SEM images (Fig. 12), raw PVP is composed of micro spheres with different size mainly in the range 1–100 μm. Soluplus was used after grinding, and the grinded soluplus is irregular particles with size mainly in the range of 10–100 μm. BM-PVP-0.5 and BM-soluplus-0.5 show the similar SEM images with irregular particles composed of small particles. PM-PVP-AH is clearly composed of QUE-AH rod-like crystals and PVP spheres. There are only a small amount of QUE-AH rod-like crystals adhering to the surface of PVP spheres. The morphology of PM-soluplus-AH is different from that of PM-PVP-AH. The surfaces of soluplus particles are fully adhered by QUE-AH rod-like crystals, indicating a strong interaction between soluplus and QUE-AH.

4. Discussion

4.1 Shortcoming of QUE metastable polymorphs

QUE-AH and QUE-AM are metastable polymorphs, which are theoretical formulation to improve the solubility of QUE. However, due to the polymorphism transformation of QUE-AH and the recrystallization of QUE-AM, they are not suitable directly as functional foods.

4.2 Shortcoming of QUE ASDs

QUE ASDs with soluplus have a strong shortcoming with the occurrence of gel-like phase separation in the dissolution process, and QUE ASDs with PVP have a weak shortcoming of the occurrence of gel-like phase separation. The existence of gel-like phase separation is the main reason for the few successful reports of QUE ASDs. Herein, the apparent solubility of PM-PVP-AH exceeds that of BM-PVP-0.5, and the apparent solubility of PM-soluplus-AH exceeds that of BM-soluplus-0.5. The ASDs prepared with PVP or soluplus as the carrier is less effective, their dissolution property is even worse than that of the PMs of QUE-AH with PVP or soluplus.

4.3 Advantages of QUE-AH PMs

The formulation of QUE in future can involve solid dispersions of metastable QUE-AH. The PMs of QUE-AH and polymers have the following advantages:

(I) No gel-like phase separation during dissolution;

(II) A relatively high degree of supersaturation;

(III) High storage stability of QUE-AH.

(IV) Selection diversity of polymers.

It can be a feasible formulation and a promising approach for QUE solubilization.

5. Conclusions

QUE ASDs with PVP or soluplus were prepared *via* neat ball milling, and their properties were compared with the PMs of QUE-AH with PVP or soluplus. BM-PVP-0.5 shows a good
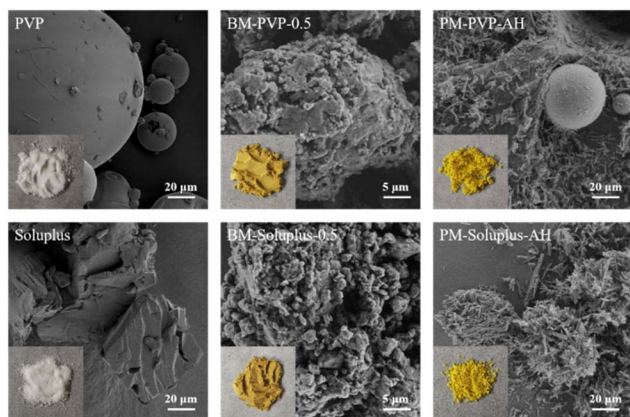

Fig. 12 Optical and SEM images of PVP, BM-PVP-0.5, PM-PVP-AH, grinded soluplus, BM-soluplus-0.5, and PM-soluplus-AH.

solubility which is little smaller than that of PM-PVP-AH. BM-soluplus-0.5 shows a poor solubility which is much smaller than that of PM-soluplus-AH. Gel-like phase separation process of QUE ASDs reduce the apparent solubility of QUE, which may be caused by the strong interactions between QUE and polymer in ASDs observed from the IR and fluorescence spectra. The PMs of metastable QUE-AH and polymer can avoid this gel-like phase separation, maintain supersaturate concentration in a high level, and have no problem of polymorphism transformation, which is a good candidate for QUE formulations. It is the first time to combine metastable QUE-AH and PMs with polymer to increase QUE solubility. Combination of metastable polymorph and polymer is a feasible strategy with low cost for improving the solubility of poorly water-soluble molecules.

Data availability

The data supporting this article have been included as part of the ESI.†

Conflicts of interest

There are no conflicts to declare.

Abbreviations

ASDs	Amorphous solid dispersions
BM-polymer-ω_{QUE} *i.e.*, BM-PVP-0.5	Ball milled quercetin and polymer
PMs	Physical mixtures
PM-polymer-quercetin polymorph *i.e.*, PM-PVP-DH	Physical mixtures of equivalent quercetin and polymer
PVP	Polyvinylpyrrolidone
QUE	Quercetin
QUE-AH	Anhydrous quercetin
QUE-AM	Amorphous quercetin
QUE-DH	Quercetin dihydrate

Acknowledgements

Notes and references

1 Q.-W. Zhang, L.-G. Lin and W.-C. Ye, *Chin. Med.*, 2018, **13**, 20.
2 Q. Lu, R. Li, Y. Yang, Y. Zhang, Q. Zhao and J. Li, *Food Chem.*, 2022, **368**, 130610.
3 N. Georgiou, M. G. Kakava, E. A. Routsi, E. Petsas, N. Stavridis, C. Freris, N. Zoupanou, K. Moschovou, S. Kiriakidi and T. Mavromoustakos, *Molecules*, 2023, **28**, 8141.
4 X. Zhu, G. Ding, S. Ren, J. Xi and K. Liu, *Food Chem.*, 2024, **458**, 140262.
5 M. H. Abraham and W. E. Acree, *J. Mol. Liq.*, 2014, **197**, 157–159.
6 E. H. Lee, *Asian J. Pharm. Sci.*, 2014, **9**, 163–175.
7 A. Paredes, P. McKenna, I. Ramoeller, Y. Naser, F. Volpe Zanutto, M. Li, M. Abbate, L. Zhao, C. Zhang, J. Abuershaid, X. Dai and R. Donnelly, *Adv. Funct. Mater.*, 2020, **31**, 1–27.
8 Y. Deng, S. Liu, Y. Jiang, I. C. B. Martins and T. Rades, *Pharmaceutics*, 2023, **15**, 2174.
9 H. Wang, P. Zhao, R. Ma, J. Jia and Q. Fu, *Drug Discovery Today*, 2024, **29**, 103883.
10 S. V. Bhujbal, B. Mitra, U. Jain, Y. Gong, A. Agrawal, S. Karki, L. S. Taylor, S. Kumar and Q. Zhou, *Acta Pharm. Sin. B*, 2021, **11**, 2505–2536.
11 M. Pisay, S. Padya, S. Mutalik and K. B. Koteshwara, *Crit. Rev. Ther. Drug Carrier Syst.*, 2024, **41**, 45–94.
12 A. Costa, F. Marquiafável, M. Leite, B. Rocha, P. Bueno, P. Amaral, H. Barud and A. Berretta, *J. Therm. Anal. Calorim.*, 2011, **104**, 273–278.
13 B. Li, S. Konecke, K. Harich, L. Wegiel, L. Taylor and K. Edgar, *Carbohydr. Polym.*, 2013, **92**, 2033–2040.
14 P. Sang Hyun, S. Im-Sook and C. Min-Koo, *Mass Spectrom. Lett.*, 2016, **7**, 79–83.
15 A. D. Gilley, H. C. Arca, B. L. B. Nichols, L. I. Mosquera-Giraldo, L. S. Taylor, K. J. Edgar and A. P. Neilson, *Carbohydr. Polym.*, 2017, **157**, 86–93.
16 X. Shi, N. Fan, G. Zhang, J. Sun, Z. He and J. Li, *Pharm. Dev. Technol.*, 2020, **25**, 472–481.
17 Y. Wang, Y. Fang, F. Zhou, Q. Liang and Y. Deng, *J. Pharm. Sci.*, 2021, **110**, 3230–3237.
18 J. Han, M. Tong, S. Li, X. Yu, Z. Hu, Q. Zhang, R. Xu and J. Wang, *Drug Dev. Ind. Pharm.*, 2021, **47**, 153–162.
19 E. Van Hecke and M. Benali, *Food Biosci.*, 2022, **49**, 101868.
20 P. Klitou, E. Parisi, S. Bordignon, F. Bravetti, I. Rosbottom, M. Dell'Aera, C. Cuocci, M. R. Chierotti, A. Altomare and E. Simone, *Cryst. Growth Des.*, 2023, **23**, 6034–6045.
21 M. S. Attia, A. Elshahat, A. Hamdy, A. M. Fathi, M. Emad-Eldin, F.-E. S. Ghazy, H. Chopra and T. M. Ibrahim, *J. Drug Delivery Sci. Technol.*, 2023, **84**, 104519.
22 W.-F. Lai and W.-T. Wong, *Crit. Rev. Food Sci. Nutr.*, 2022, **62**, 7319–7335.
23 G. S. Borghetti, J. P. Carini, S. B. Honorato, A. P. Ayala, J. C. F. Moreira and V. L. Bassani, *Thermochim. Acta*, 2012, **539**, 109–114.
24 Z. Jurasekova, A. Torreggiani, M. Tamba, S. Sanchez-Cortes and J. V. Garcia-Ramos, *J. Mol. Struct.*, 2009, **918**, 129–137.
25 K. Srinivas, J. W. King, L. R. Howard and J. K. Monrad, *J. Food Eng.*, 2010, **100**, 208–218.
26 R. S. Razmara, A. Daneshfar and R. Sahraei, *J. Chem. Eng. Data*, 2010, **55**, 3934–3936.
27 D. Althans, P. Schrader and S. Enders, *J. Mol. Liq.*, 2014, **196**, 86–93.
28 L. Chebil, C. Chipot, F. Archambault, C. Humeau, J. M. Engasser, M. Ghoul and F. Dehez, *J. Phys. Chem. B*, 2010, **114**, 12308–12313.
29 D. Krishna Sandilya and A. Kannan, *Ultrason. Sonochem.*, 2010, **17**, 427–434.

30 D. Csicsák, E. Borbás, S. Kádár, P. Tőzsér, P. Bagi, H. Pataki, B. Sinkó, K. Takács-Novák and G. Völgyi, *New J. Chem.*, 2021, **45**, 11618–11625.

31 M. Haripada, K. Cyrus and D. Juan, *Curr. Pharm. Biotechnol.*, 2009, **10**, 609–625.

32 M. Buchweitz, P. A. Kroon, G. T. Rich and P. J. Wilde, *Food Chem.*, 2016, **211**, 356–364.

33 J. Hanuza, P. Godlewska, E. Kucharska, M. Ptak, M. Kopacz, M. Mączka, K. Hermanowicz and L. Macalik, *Vib. Spectrosc.*, 2017, **88**, 94–105.

34 P. J. Larkin, M. Dabros, B. Sarsfield, E. Chan, J. T. Carriere and B. C. Smith, *Appl. Spectrosc.*, 2014, **68**, 758–776.

35 Y. Numata and H. Tanaka, *Food Chem.*, 2011, **126**, 751–755.

36 S. C. Uyeki, C. M. Pacheco, M. L. Simeral and J. H. Hafner, *J. Phys. Chem. A*, 2023, **127**, 1387–1394.

37 T. He, N. Niu, Z. Chen, S. Li, S. Liu and J. Li, *Adv. Funct. Mater.*, 2018, **28**, 1706196.

38 T. Prutskij, A. Deriabina, F. J. Melendez, M. E. Castro, L. Castillo Trejo, G. D. Vazquez Leon, E. Gonzalez and T. S. Perova, *Chemosensors*, 2021, **9**, 315.